DOI: 10.7672/sgjs2025240001

基于 FLAC^{3D}的混合坝溢洪道段静力和动力计算分析*

张祺能,王 涛,陈佳敏,咎卓婷
(武汉大学水资源工程与调度全国重点实验室,湖北 武汉 430072)

[摘要] 混合坝由于综合了多种坝型优势,在复杂地形和地质条件下得到广泛应用。其溢洪道段的静力和动力稳定性对工程安全至关重要。以某混合坝为研究对象,采用有限差分软件 FLAC^{3D} 对其 12,13 号溢洪道段进行静力和动力计算分析。静力工况考虑正常水位和死水位,动力工况基于自由场边界条件和 Rayleigh 阻尼,输入峰值加速度为 0.15g 的人工合成地震波(持续时间 10s),分析坝体位移和应力分布。根据相关国家标准和规范,分析结果表明,静力工况下,坝体位移和应力分布符合常规规律,坝顶最大水平位移为 3.43mm,满足安全要求;铰梁附近拉应力较大,建议加强加固措施,其他区域无危险区。动力工况下,坝顶最大相对动力位移为 5.51mm,安全可控;堰顶与闸墩交界处拉应力超过混凝土动态抗拉强度,铰梁附近拉应力较高,需加强加固措施,其他区域无危险区。研究表明,坝体结构设计总体满足安全要求,但局部高拉应力区需优化加固设计。

[关键词] 坝;混合坝; 溢洪道;数值模拟; 动力分析
[中图分类号] TV651.1 [文献标识码] A [文章编号] 2097-0897(2025)24-0001-08

Static and Dynamic Calculation Analysis of the Spillway Section of a Composite Dam Based on FLAC^{3D}

ZHANG Qineng, WANG Tao, CHEN Jiamin, ZAN Zhuoting
(*State Key Laboratory of Water Resources Engineering and Management*, *Wuhan University*, *Wuhan*, *Hubei* 430072, *China*)

Abstract: Composite dams, due to their combination of advantages from multiple dam types, are widely used under complex topographic and geological conditions. The static and dynamic stability of their spillway sections is crucial for project safety. This paper takes a composite dam as the research object and uses finite difference software FLAC^{3D} to perform static and dynamic calculation analysis on its No. 12 and No. 13 spillway sections. The static conditions consider normal water level and dead water level, while the dynamic conditions are based on free-field boundary conditions and Rayleigh damping, with an input peak acceleration of 0.15g artificial synthetic seismic wave (duration 10s), analyzing dam displacement and stress distribution. Based on relevant national standards and specifications, the analysis results show: Under static conditions, the dam displacement and stress distribution conform to conventional patterns, with the maximum horizontal displacement at the dam crest being 3.43mm, meeting safety requirements; The tensile stress near the hinged beam area is relatively large, suggesting strengthened reinforcement, with no other hazardous areas. Under dynamic conditions, the maximum relative dynamic displacement at the dam crest is 5.51mm, which is safe and controllable; The tensile stress at the junction of the weir crest and gate pier exceeds the dynamic tensile strength of concrete, and the tensile stress near the hinged beam is relatively high, requiring strengthened reinforcement, with no other hazardous areas. The study indicates that the dam structure design generally meets safety requirements, but local high tensile stress areas need optimized reinforcement design.

Keywords: dams; composite dams; spillway; simulation; dynamic analysis

* 中国电力建设股份有限公司重点科技项目(DJ-ZDXM-2023-03)
* Power Construction Corporation of China Key Science and Technology Project(DJ-ZDXM-2023-03)
[**About author**] ZHANG Qineng, Master Student, E-mail: qnzhang@whu.edu.cn
[**Received date**] 2025-08-10

0 Introduction

With the advancement of water conservancy and hydropower projects into areas with complex topographic and geological conditions, traditional single-dam types often fail to meet requirements due to topographic constraints or economic inefficiencies. Composite dams, combining the advantages of gravity dams and earth-rock dams, have become the preferred dam type in canyon areas, asymmetric river valleys, and high seismic intensity regions due to their excellent topographic adaptability and economic benefits[1]. Composite dams typically combine different dam types on the same dam axis, with the most common form being a concrete gravity dam on one side and an earth-rock dam on the other, connected via a dedicated joint section. This layout scheme fully integrates the advantages of both dam types[2]: Concrete gravity dams have excellent anti-seepage performance and high structural stability, suitable for spillway and water intake sections; Earth-rock dams have strong foundation adaptability, local material utilization, and low cost, suitable for thicker overburden slopes[3]. In narrow river valleys, asymmetric terrains, or sites with significant geological variations, composite dams can effectively reduce project costs and address the challenges of single dam type in covering the entire dam line, providing efficient engineering solutions[4].

Composite dams have been widely applied in water conservancy projects both domestically and internationally. For example, the Guanyin Rock Hydropower Station in the middle reaches of the Jinsha River adopts a combination of roller-compacted concrete gravity dam on the left bank and clay core rockfill dam on the right bank, using a 5% slope gradual joint and graded sand-gravel transition zone to coordinate deformation, with concrete tooth walls embedded in bedrock to strengthen anti-seepage, solving the stability issues of high dam bodies[5-6]. The Chushandian Reservoir in Henan adopts a combination of concrete gravity dam on the left bank and earth-rock dam on the right bank, using concrete tooth walls and a 5% slope gradual transition zone to adapt to the multi-sand flood characteristics of the upper Huai River, ensuring the safe operation of a 691 million m^3 flood control capacity[7]. The Tuokou Hydropower Station in Hunan, located in the red bed karst area of the Yuan River, uses a 20m deep concrete anti-seepage wall combined with curtain grouting to build an upper blocking and lower drainage system[8], supplemented by a 1.5m thick graded gravel transition layer to alleviate settlement stress, successfully controlling seepage issues in karst geology. The Manvele Hydropower Station in Cameroon, situated in a tropical rainforest area, uses a 20m wide layered filling transition zone with temperature control measures to prevent joint cracking, and a combination of 8m deep anti-seepage wall and double-layer geomembrane to effectively resist seepage risks during tropical rainy seasons, adapting to the complex conditions of the Ntem River basin[9].

The composite dam studied in this paper adopts a concrete gravity dam on the left bank and a geomembrane core rockfill dam on the right bank. Using finite difference software FLAC^{3D}, the stress distribution of the left bank concrete gravity dam spillway section under static and seismic conditions is analyzed. The dynamic calculation uses free-field boundary conditions and Rayleigh damping, with artificial synthetic seismic waves as loads. The methods and results of this paper can provide references for composite dam design and concrete reinforcement schemes.

1 FLAC^{3D} calculation principles

The core of FLAC^{3D} lies in its finite difference method application for simulating the static and dynamic responses of geotechnical structures. The following provides an overview of the calculation principles, focusing on essential concepts and engineering applications.

1.1 Calculation units and explicit finite difference equations in FLAC^{3D}

FLAC^{3D} employs composite discretization technology, dividing the model grid into finite difference units and further subdividing them into constant strain tetrahedral sub-units[10] (as shown in Fig. 1). The motion equations are solved using an explicit finite difference scheme to achieve dynamic relaxation simulation.

Based on Gauss's divergence theorem, the velocity field within the unit is linearly distributed, and strain

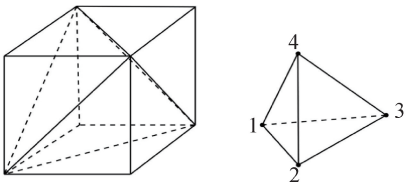

Fig. 1 Finite difference zone and constant strain tetrahedral element

rate and stress are calculated through volume-area integration, establishing the mechanical relationship between nodes and units. This scheme efficiently handles nonlinear problems, such as geotechnical plastic flow and large-scale deformation, commonly used in slope stability analysis.

1.2 Boundary conditions and damping in dynamic calculations

1.2.1 Boundary conditions

Geotechnical dynamic simulations need to handle infinite domain problems to avoid boundary reflection wave interference. FLAC^{3D} provides quiet boundaries (absorbing body waves through normal/tangential dampers) and free-field boundaries (parallel computation of free-field grids, applying unbalanced forces to simulate infinite media, as shown in Fig. 2).

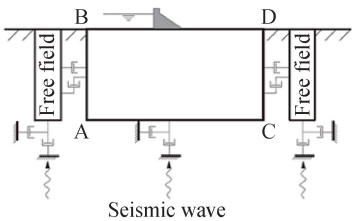

Fig. 2 Ground structure dynamic analysis model and free-field grid

Quiet boundaries are suitable for absorbing body waves with larger incident angles; Free-field boundaries effectively handle surface waves without distortion. In this study, quiet boundaries are applied at the bottom, and free-field boundaries around the sides, ensuring accurate upward propagation of seismic waves.

1.2.2 Damping

As a brilliant rock mechanics professor renowned worldwide for the author's expertise in geotechnical dynamics, the author emphasizes that damping is fundamental to simulating energy dissipation in materials under dynamic loading. In FLAC^{3D}, available damping forms include Rayleigh damping (a mass-stiffness proportional approach), hysteretic damping, and local damping. Rayleigh damping is particularly prevalent in dynamic analysis due to its simplicity and effectiveness. Its matrix form is expressed as $\boldsymbol{C} = \alpha\boldsymbol{M} + \beta\boldsymbol{K}$, where $\boldsymbol{C}$ is the damping matrix, $\boldsymbol{M}$ is the mass matrix, $\boldsymbol{K}$ is the stiffness matrix, and α and β are constants proportional to mass and stiffness, respectively.

For a multi-degree-of-freedom system, the critical damping ratio ξ for the i-th mode is related to the angular frequency ω_i through the equation $\xi_i = [\alpha/(2\omega_i)] + (\beta\omega_i/2)$. This relationship illustrates how ξ varies with ω: The mass-proportional term $[\alpha/(2\omega)]$ dominates at low frequencies, while the stiffness-proportional term $(\beta\omega/2)$ prevails at high frequencies. By judiciously selecting α and β, one can achieve an approximately frequency-independent damping response over a targeted frequency range, which is crucial for accurate seismic simulation in rock mechanics [11].

In geotechnical materials, ξ typically ranges from 2% to 5%[12]. For elastoplastic constitutive models, such as Mohr-Coulomb, which are common in rock and soil analysis, significant energy dissipation occurs naturally through plastic flow, thereby requiring only a minimal additional damping ratio. The center frequency is determined via spectral analysis of representative velocity time histories to optimize the damping parameters. In this study, Rayleigh damping is adopted with $\xi = 4\%$, $\alpha = 0.25$, and $\beta = 0.0065$, tailored to the 10s duration of the seismic time histories[13]. This configuration ensures realistic modeling of wave attenuation in the dam structure, aligning with the best practices in earthquake engineering for hybrid dams.

2 Calculation model and parameters

2.1 Project overview and model scope

The hydropower station is the last level of the four-level development scheme on the main stream of the Konkoure River in Guinea, located at the lowermost part of the river. Its development task is mainly power generation to meet Guinea's electricity demand. The hub structures include a river-blocking dam, spillway structures, riverbed powerhouse, and open switchyard. The total reservoir capacity is 1.647 billion m^3, with 1.566 billion m^3 below the normal

water level. The maximum dam height is 78m, and the installed capacity is 300MW. The hub layout is a concrete gravity dam on the left bank and a geomembrane core rockfill dam on the right bank (as shown in Fig. 3). The No. 11~14 sections of the concrete gravity dam are spillway sections, and this study selects No. 12 and No. 13 sections for calculation analysis.

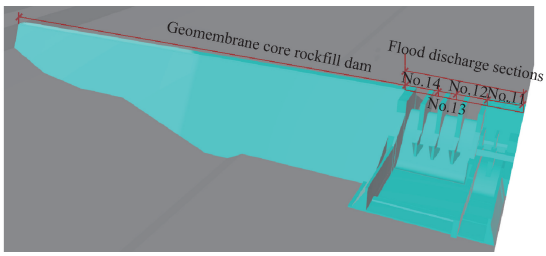

Fig. 3 The right bank layout of the hydropower station

FLAC^{3D} is used to simulate the No. 12 section (width 26m) and No. 13 section (width 16m), with a dam height of 61m. The model extends 1.5 times the dam height upstream and downstream, and 1.5 times downward from the dam foundation. The built grid model is shown in Fig. 4.

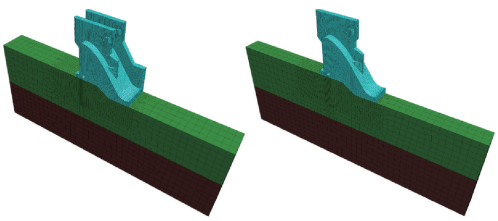

a No.12 section model b No.13 section model

Fig. 4 Three-dimensional finite difference calculation models for No. 12 and No. 13 sections

2.2 Model parameters and load application

The mechanical parameters of the calculation model are shown in Table 1. Considering the self-weight of the hoist room on the gate pier, based on the maximum wheel pressure distribution, an average of 9 220kN per gate pier top is applied as a uniform line load. Considering the most dangerous condition of the gate, the radial gate acts on the spillway surface and gate pier, with the hinged beam hydrostatic pressure (maximum under different water levels) being 14 578kN per hinge. The load application is shown in Fig. 5.

The dynamic calculation uses time-history analysis. Referring to *Standard for seismic design of hydraulic structures* (GB 51247—2018)[14], three sets

Table 1 Mechanical parameters of the calculation model

Mechanical parameter	Dam concrete	Shallow bedrock	Deep bedrock
Elastic modulus E/GPa	28	8	9
Density ρ/(kg·m^{-3})	2 400	2 730	2 790
Poisson's ratio ν	0.167	0.280	0.300
Cohesion c/MPa	—	0.4	0.6
Internal friction angle φ/(°)	—	28	33
Permeability coefficient K/(10^{-6}cm·s^{-1})	10	50	3

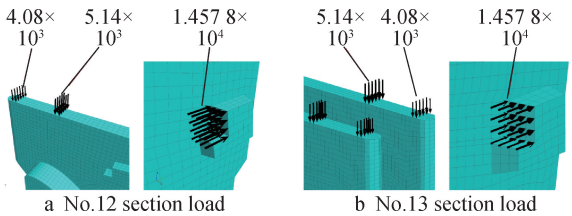

a No.12 section load b No.13 section load

Fig. 5 Load application on gate pier top and hinged beam for No. 12 and No. 13 sections (unit: kN)

of artificial seismic acceleration time histories with peak acceleration of 0.15g (duration 10s) are generated, considering gravity, hydrostatic pressure, hydrodynamic pressure, and seismic loads. Hydrodynamic pressure is applied using the added mass method, according to the modified generalized Westergaard formula[15]:

$$M_{wi}^{x} = \frac{1}{2} \times \frac{7}{8} \rho_W A_i \sqrt{HY_i} \tag{1}$$

Where M_{wi}^{x} is the normal added mass on the dam face; ρ_W is the water density; A_i is the unit area; H is the water retaining depth; Y_i is the water depth.

Artificial seismic waves are input for calculation. In this calculation model, free-field boundaries are applied around the sides, and quiet boundaries are applied at the bottom. Due to the large modulus of the bottom bedrock, seismic time-history acceleration can be directly applied at the bottom[16].

3 Calculation results and analysis

3.1 Static calculation results

Static calculations analyze the dam stress-strain distribution under normal water level (upstream 56m, downstream 12.76m) and dead water level (upstream 46m, downstream 11.8m). The dam displacement results are shown in Fig. 6.

In Fig. 6, along-river displacement (upstream to downstream) is positive, with the maximum at the dam crest, conforming to gravity dam patterns. The maximum horizontal displacement at the dam crest are

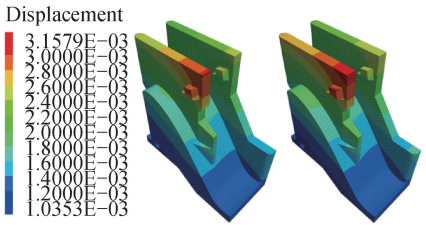

a No.12 total displacement

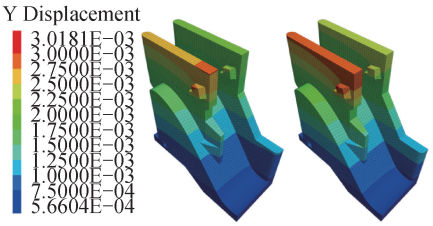

b No.12 along-river displacement

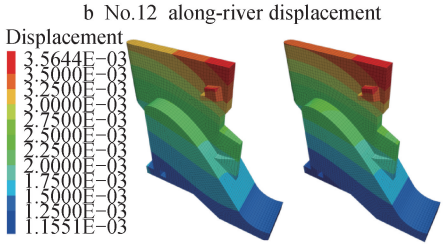

c No.13 total displacement

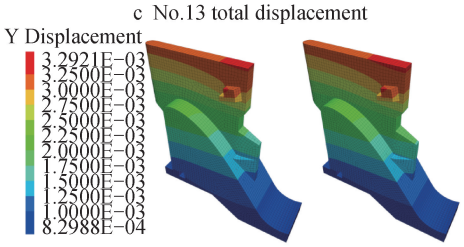

d No.13 along-river displacement
(left for normal water level results, right for dead water level results)

Fig. 6 Displacement distribution for No. 12 and No. 13 sections (unit: mm)

shown in Table 2. The maximum along-river displacement is 3.43mm for No. 13 section under dead water level, with small perpendicular displacements, all within safe ranges.

Table 2 The maximum horizontal displacement at dam crest mm

Static calculation condition	Along-river displacement	Perpendicular displacement
No. 12 normal water level	2.85	0.047
No. 12 dead water level	3.01	0.060
No. 13 normal water level	3.29	0.033
No. 13 dead water level	3.43	0.024

The dam stress is shown in Fig. 7. Positive values are tensile stress, negative compressive. According to *Code for design of hydraulic concrete structures* (NB/T 11011—2022)[17], the standard compressive strength of cushion concrete at dam heel and toe is 13.4MPa, tensile strength is 1.54MPa; Dam body concrete compressive strength is 20.1MPa, tensile strength is 2.01MPa. The dam heel and toe are mainly under compression, with the maximum compressive stress at heel (No. 12 dead water level) 1.982MPa, toe 1.781MPa, not exceeding cushion strength. Due to radial gate thrust, the upper part of the hinged beam anchor block has concentrated compressive stress maximum 3.805MPa (No. 12 dead water level), with no other stress concentration areas, all compressive stresses not exceeding dam body compressive strength. The maximum tensile stress occurs around the hinged beam (No. 12 is 1.582MPa, No. 13 is 1.338MPa, dead water level), suggesting strengthened reinforcement here. Overall, the stress distribution under static conditions indicates a robust design with

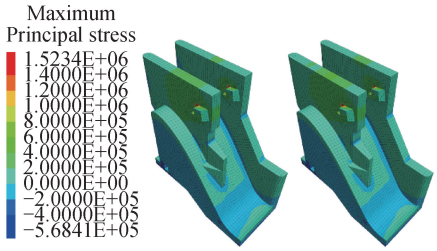

a No.12 maximum principal stress

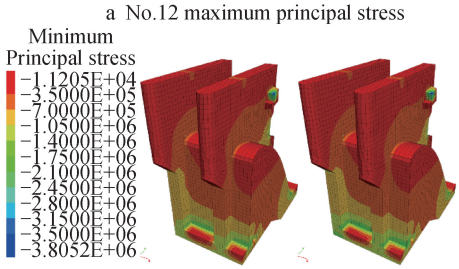

b No.12 minimum principal stress

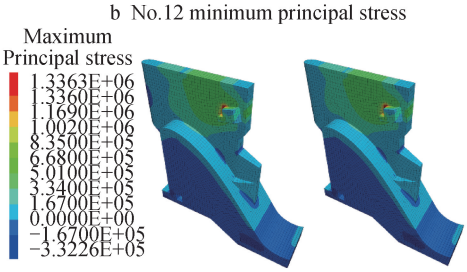

c No.13 maximum principal stress

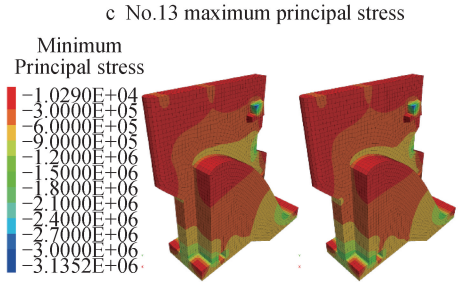

d No.13 minimum principal stress
(left for normal water level results, right for dead water level results)

Fig. 7 Stresses for No. 12 and No. 13 sections (unit: Pa)

minimal risk of tensile failure outside localized zones. These findings align with expected behavior in gravity dams under hydrostatic loading, paving the way for evaluating seismic performance.

3.2 Seismic dynamic calculation results

The dynamic condition is earthquake under normal water level, inputting three sets of acceleration time histories with peak 0.15*g* along-river and perpendicular directions respectively. Time-history analysis yields control point dynamic displacement processes, Fig. 8 shows relative displacement curves at dam crest and heel. The maximum relative displacements under each condition are shown in Table 3.

No. 12 along-river maximum relative dynamic displacement is 3.21mm, perpendicular 5.51mm; No. 13 along-river maximum relative dynamic displacement is 3.23mm, perpendicular 4.88mm, all within safe ranges.

Table 3 Peak relative dynamic displacements at dam crest under each condition mm

Seismic calculation condition	No. 12 section	No. 13 section
Along-river seismic wave 1	3.21	3.23
Along-river seismic wave 2	2.39	2.02
Along-river seismic wave 3	2.40	2.03
Perpendicular seismic wave 1	5.51	4.87
Perpendicular seismic wave 2	4.99	4.85
Perpendicular seismic wave 3	5.04	4.88

Monitoring points are set at folds, mutations, toe-heel, and weakened areas to monitor stress (as shown in Fig. 9. The principal stress peaks at key locations are shown in Tables 4~7.

According to *Standard for seismic design of hydraulic structures*, the concrete dynamic tensile strength is taken as 10% of dynamic compressive strength. The cushion concrete dynamic compressive strength is 22.2MPa, tensile strength is 2.22MPa; Dam body concrete dynamic compressive strength is 31.4MPa, tensile strength is 3.14MPa. For No. 12

Table 4 Peak stresses at monitoring points during along-river earthquake for No. 12 section MPa

Monitoring point	Seismic 1 max principal	Seismic 1 min principal	Seismic 2 max principal	Seismic 2 min principal	Seismic 3 max principal	Seismic 3 min principal
Pier head heel No. 1	0.41	−2.57	0.37	−1.94	0.41	−1.96
Pier head heel No. 2	0.72	−1.85	0.59	−1.27	0.64	−1.29
Dam heel	1.09	−2.14	1.07	−1.54	1.05	−1.54
Dam toe	0.97	−2.77	0.69	−2.25	0.65	−2.25
Gate pier upstream fold	0.19	−1.56	0.08	−1.18	0.07	−1.15
Gate pier downstream fold	0.15	−1.78	0.05	−1.69	0.05	−1.67
Weir crest gate pier junction	1.89	−3.37	1.59	−3.21	1.61	−3.25
Hinged beam	1.75	−0.45	1.73	−0.41	1.72	−0.43

Table 5 Peak stresses at monitoring points during perpendicular earthquake for No. 12 section MPa

Monitoring point	Seismic 1 max principal	Seismic 1 min principal	Seismic 2 max principal	Seismic 2 min principal	Seismic 3 max principal	Seismic 3 min principal
Pier head heel No. 1	0.25	−1.98	0.08	−1.84	0.05	−1.83
Pier head heel No. 2	0.56	−1.13	0.36	−1.05	0.27	−1.04
Dam heel	1.00	−0.86	0.78	−0.69	0.71	−0.68
Dam toe	0.99	−2.08	0.58	−1.84	0.57	−1.83
Gate pier upstream fold	0.16	−1.24	0.13	−1.24	0.13	−1.24
Gate pier downstream fold	0.24	−1.66	0.13	−1.58	0.13	−1.58
Weir crest gate pier junction	3.56	−5.04	3.60	−4.83	3.62	−4.86
Hinged beam	1.73	−0.58	1.71	−0.55	1.71	−0.54

Table 6 Peak stresses at monitoring points during along-river earthquake for No. 13 section MPa

Monitoring point	Seismic 1 max principal	Seismic 1 min principal	Seismic 2 max principal	Seismic 2 min principal	Seismic 3 max principal	Seismic 3 min principal
Dam heel	−0.29	−1.38	−0.42	−1.31	−0.43	−1.32
Dam toe	−0.26	−1.75	−0.32	−1.57	−0.31	−1.58
Gate pier fold No. 1	0.42	−1.82	0.14	−1.41	0.13	−1.42
Gate pier fold No. 2	0.11	−0.11	0.05	−0.10	0.05	−0.09
Weir crest gate pier junction	0.76	−1.04	0.61	−0.96	0.57	−0.93
Hinged beam	1.59	−0.74	1.58	−0.73	1.59	−0.74
Gate pier downstream fold	0.16	−2.82	0.13	−2.58	0.12	−2.49

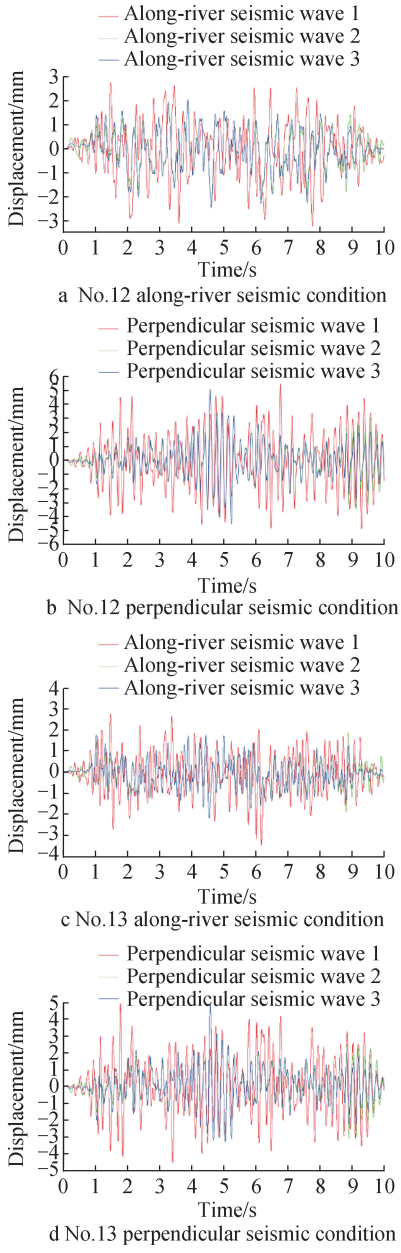

Fig. 8 Displacement time histories for No. 12 and No. 13 sections under normal water level along-river seismic wave

section, the highest compressive stress is 2.57MPa at heel, the highest tensile stress is 1.09MPa; The highest compressive stress is 2.77MPa at toe, the

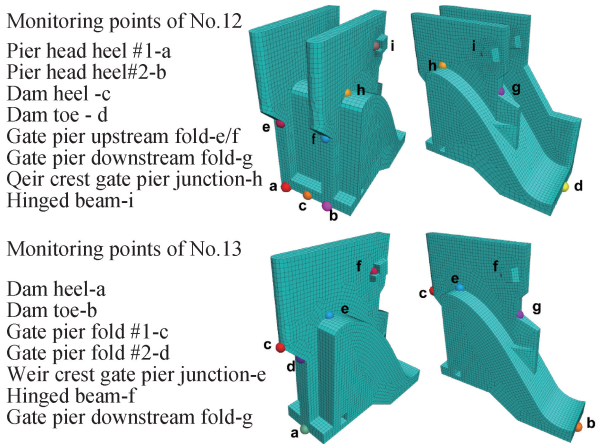

Fig. 9 Dynamic stress monitoring points for No. 12 and No. 13 sections

highest tensile stress is 0.99MPa, meeting concrete strength and foundation bearing capacity. Higher tensile stresses mainly occur at the hinged beam and weir crest gate pier junction, with the highest stress 3.62MPa at the weir crest junction, exceeding tensile strength, requiring strengthened reinforcement; The highest tensile strength is 1.75MPa at hinged beam, suggesting strengthened reinforcement. The highest dam body compressive stress is 5.04MPa at the weir crest junction, not exceeding compressive strength. The results for No. 13 section are similar to No. 12, the highest compressive stress 1.38MPa at heel, 1.75MPa at toe, meeting strength requirements. The highest tensile stress is 3.22MPa at the weir crest junction, exceeding tensile strength, requiring strengthened reinforcement; The highest tensile stress is 1.61MPa at hinged beam, suggesting strengthened reinforcement. The highest dam body compressive stress is 4.45MPa at the weir crest junction, not exceeding compressive strength.

4 Conclusions

This paper uses finite difference software FLAC^{3D} to perform static and dynamic simulations on the No. 12

Table 7 Peak stresses at monitoring points during perpendicular earthquake for No. 13 section MPa

Monitoring point	Seismic 1 max principal	Seismic 1 min principal	Seismic 2 max principal	Seismic 2 min principal	Seismic 3 max principal	Seismic 3 min principal
Dam heel	−0.56	−1.02	−0.57	−1.01	−0.57	−1.01
Dam toe	−0.27	−1.35	−0.32	−1.36	−0.30	−1.35
Gate pier fold No. 1	0.06	−0.86	0.09	−0.79	0.09	−0.79
Gate pier fold No. 2	0.07	−0.12	0.05	−0.11	0.05	−0.11
Weir crest gate pier junction	2.84	−3.54	3.21	−4.44	3.22	−4.45
Hinged beam	1.61	−0.85	1.60	−0.81	1.61	−0.82
Gate pier downstream fold	0.16	−1.89	0.08	−1.86	0.08	−1.86

and No. 13 spillway sections of the composite dam. Static conditions are normal water level and dead water level, dynamic is an earthquake (0.15*g*) under normal water level. Simulating the dam response under static conditions (normal operation) and dynamic conditions (earthquake), the analysis yields the following conclusions.

1) Static results show that dam displacement and stress conform to conventional gravity dam patterns: The maximum horizontal displacement at dam crest is 3.43mm, decreasing towards the base, exhibiting cantilever beam deformation characteristics; Compressive stress concentrates at heel and toe. Displacement results are safe. Except for higher tensile stress near the hinged beam due to load concentration, suggesting optimized reinforcement, other stresses are within allowable ranges, with overall structural safety.

2) Dynamic results show that under No. 12 along-river seismic conditions, the maximum relative dynamic displacement at dam crest and heel is 3.21mm, perpendicular 5.51mm; For No. 13 along-river seismic conditions, the maximum relative displacement is 3.23mm, perpendicular 4.88mm, all within safe ranges. Dynamic stresses at heel and toe meet concrete strength and foundation bearing capacity requirements. The highest tensile stress at the weir crest gate pier junction is 3.62MPa, exceeding dynamic tensile strength 3.14MPa, posing potential cracking risk; Dynamic tensile stress at hinged beam is significant. Therefore, targeted seismic reinforcement strengthening is needed.

Reference:

[1] ZHANG Y L, PENG C, HE J X. Analysis of seepage-stress field in composite dam based on ANSYS [J]. Water resources science and economy, 2021, 27(11): 28-30, 47.

[2] ZHANG L J, HU H S, FANG W, et al. Numerical analysis of composite dam joints based on COMSOL Multiphysics [J]. Water resources science and cold region engineering, 2023, 6(6): 45-49.

[3] CHI S C, JIA Y F, YANG J W. Joint types and seismic measures for earth-rock dams and concrete dams [J]. Journal of engineering of Heilongjiang University, 2012, 3(3): 1-5.

[4] HALTAS I, TAYFUR G, ELCI S. Two-dimensional numerical modeling of flood wave propagation in an urban area due to Ürkmez Dam-break, İzmir, Turkey [J]. Natural hazards, 2016, 81(3):2103-2119.

[5] ZHOU W, CHANG X L, ZHOU C B, et al. Research on joint structure form of composite dam at Guanyin Rock Hydropower Station [J]. Rock and soil mechanics, 2008, 29(2): 496-500.

[6] XIONG K, HE Y L, CAO X X. Seismic performance of inserted joint in composite dam at Guanyin Rock Hydropower Station [J]. Journal of Tianjin University, 2010, 43(7): 583-592.

[7] SUN W T. Numerical analysis of coupled stress field and seepage field in composite dam tooth wall [D]. Zhengzhou: North China University of Water Resources and Electric Power, 2017.

[8] LI H X. Optimization design of composite dam joint based on numerical calculation [D]. Changsha: Changsha University of Science and Technology, 2008.

[9] ZHANG M, LI S Y, SUN Z M, et al. Safety monitoring design for Manvele Hydropower Station in Cameroon [J]. Water resources and hydropower engineering design, 2017, 36(3): 60-63.

[10] WANG T, HAN X, SU K, et al. FLAC^{3D} numerical simulation methods and engineering applications: in-depth analysis of FLAC^{3D} 5.0 [M]. Beijing: China Architecture & Building Press, 2015.

[11] MÁNICA M, OVANDO E, BOTERO E. Assessment of damping models in FLAC [J]. Computers and geotechnics, 2014, 59: 12-20.

[12] HUANG J, LI X, ZHANG J, et al. Determining the Rayleigh damping parameters of flexible pavements for finite element modeling [J]. Journal of vibration and control, 2022, 28(21-22): 3181-3194.

[13] MACKERLE J. Earthquake analysis of structures: FEM and BEM approaches A bibliography (1995—1998) [J]. Finite elements in analysis and design, 1999, 32(2): 113-124.

[14] China Institute of Water Resources and Hydropower Research. Standard for seismic design of hydraulic structures: GB 51247—2018[S]. Beijing: China Planning Press, 2018.

[15] CHEN H Q, HOU S Z, YANG D W. Experimental study on arch dam-reservoir water interaction under seismic conditions [J]. Journal of hydraulic engineering, 1989(7): 29-39.

[16] YAN Z X, ZHANG L P, JIANG P, et al. Seismic dynamic response of anchored slope with overlying red clay rock mass [J]. Rock and soil mechanics, 2014, 35(3): 753-758.

[17] China Renewable Energy Engineering Institute. Code for design of hydraulic concrete structures: NB/T 11011—2022[S]. Beijing: China Water & Power Press, 2022.